



FRACTOGRAPHIC OBSERVATIONS OF DELAMINATION GROWTH MECHANISMS

Emile S Greenhalgh*, Charlotte Rogers*, Paul Robinson*
***The Composite Centre, Imperial College, London, UK**

Keywords: *Delamination, fractography, micro-mechanisms, failure criteria, shear*

Abstract

This paper provides an overview of fractographic observations from the detailed examination of delamination fracture surfaces. Firstly, the relationship between toughness, delamination failure criteria and fracture morphology is presented and the influence on toughness of cusp formation and deformation is discussed. Recent research is presented on macromodelling of cusps using shear loaded PVC foam. Delamination migration at multidirectional ply interfaces is then discussed and the mechanism by which delaminations migrate is presented. It is demonstrated how migration can be avoided in fracture toughness coupons and consequently the toughness of multidirectional ply interfaces can be characterised. The influence of migration on delamination growth from embedded defects in laminates under compression is presented, and these results are extended to demonstrate how migration influences damage growth in structures. The paper concludes by making recommendations for realistic modelling of migration, and suggests how it can be exploited in damage tolerant structural design.

1 Introduction

Delamination is the Achilles' heel of composites and there have been considerable efforts to address the issues associated with it. Modelling of delamination has proved to be computationally demanding and early efforts made considerable simplifications which led to poor predictions [1]. Consequently, the certification authorities now require extensive structural testing to demonstrate tolerance to delamination. Current predictive models have much greater computational resources at their disposal and improved methods, such as interface elements [2]. However, to be reliable, such models still need to base their formulation on realistic

damage processes. A vital tool to achieve this is *fractography*; examination of the fracture surfaces to deduce the detailed failure mechanisms. This offers a comprehensive insight into the mechanisms by which delaminations grow, and thus provides models with a basis upon which to predict damage growth and structural failure. This paper describes observations from the detailed examination of delamination fracture surfaces and relates these to toughness and delamination growth behaviour in structures. The aim is to provide an overview of the understanding of delamination which has been developed through fractographic observations. Finally, based on these observations, recommendations are made regarding delamination modelling and damage tolerant design.

2 Delamination Toughness and Failure Criteria

The recognized approach [1] to characterising delamination has been to determine the toughness under controlled combinations of modes I (peel), II (shear) and III (tearing). This generates a delamination failure locus (toughness versus mode mixity), the magnitude and shape of which is influenced by factors such as moisture, temperature and ply orientation. This locus is modelled, often empirically, to produce a delamination failure criterion [3]. There many proposed failure criteria, ranging from those with an empirical basis to some which have considered physical failure mechanisms.

The delamination failure locus for Hexcel T800/924 (a carbon-fibre/modified epoxy) is shown in Fig. 1. Also illustrated are images of the fracture morphologies at different mode-mixities. Delamination toughness can be attributed to a combination of different micromechanisms. The changes in morphology in Fig. 1 directly reflect the changes in fracture mechanisms which contribute to the delamination toughness. Under mode I loading composites exhibit the lowest toughness (Fig. 2a) and matrix cleavage (cohesive fracture) is the main contributor to the toughness. In toughened matrix

systems which contain thermoplastic phases, the matrix is more ductile leading to a larger process zone and improvements in the mode I toughness. As the mode II component increases, the toughness increases, which is principally attributed to the formation of cusps (Fig. 2b). Macroscopically, this appears as an increase in surface roughness, as can be seen in Fig. 1. On a microscopic level, cusps form by the development of angled cracks at the interply resin region, and angle of which depends upon the mode-mixity [1]. As the mode II component increases, the incidence and inclination of the cracks increases and thus so does the fractured area generated. These angled cracks extend towards the plies and coalesce. Locally, the formation of the cusps is cleavage fracture, leading to an overall increase in fracture energy absorption and toughness as the mode II component increases.

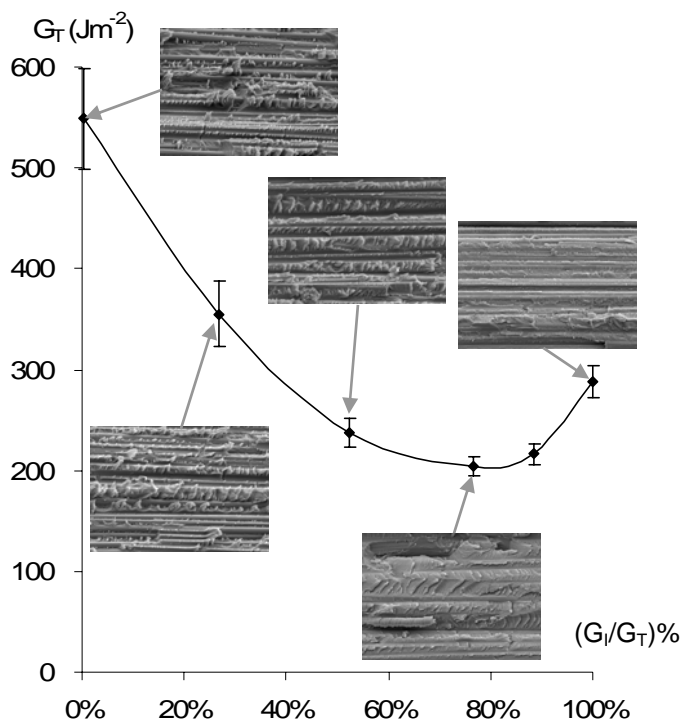
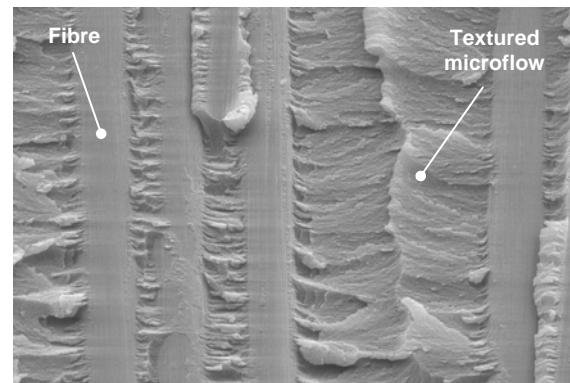


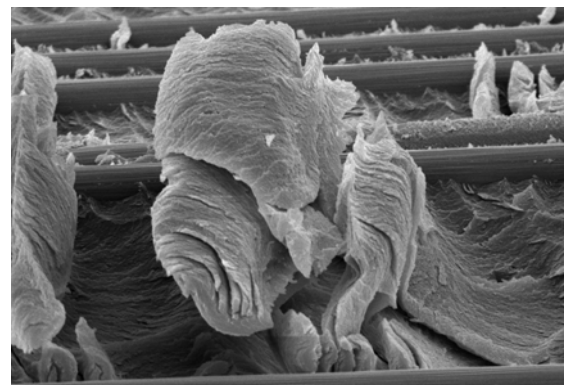
Fig. 1 Toughness versus mode mixity for T800/924 showing the change in fracture morphology (x500)

A number of researchers have considered the formation of angled cracks in brittle solids and the contribution they make to the material toughness [4,5]. These have been extended to proposed delamination failure criteria which model the contribution that cusps make to the toughness by relating them to the overall area of fracture [1,3,6]. These criteria only hold if there is no plastic deformation of the resin, and thus assume brittle resin fracture. O'Brien [7] extended this idea by

suggesting that G_{IIC} can be derived by considering the local G_{IC} toughness of the resin; the apparent increase in toughness as the mode II component increases (Fig. 1) is attributed to the increase in fracture area via cusp formation. Consequently G_{IIC} is not a material property, and a delamination failure criterion can be derived purely from the G_I contribution. This has been further extended by Kinloch *et al* [8] who proposed that a crack loaded globally under mixed mode loading would fail when the induced mode-I component reaches a critical value. This assumes that a mechanism, such as 'surface roughness', results in part by the mode-II SERR being controlled by a mode-I component.



(a) Mode I fracture in T800/924 (x2k)



(b) A cusp in mode II fracture in T800/924 (x2k)

Fig. 2 Micro-mechanisms which contribute to delamination toughness

Since cusp development is the principal contribution to the mode II and mixed-mode toughness of thermoset composites, an understanding of the cusp formation processes should lead to a physically based failure criterion. However, the small scale of these features makes in-situ characterisation problematic. An alternative approach is to simulate the cusp formation at a macroscale. This approach has proved to have been productive in the past for understanding the fracture

behaviour of composites. For example, Jelf and Fleck [9] modelled fibre microbuckling using dental wax and spaghetti. It has been observed that shear testing of polymer foam [10] generates cusps which are identical to those in CFRP (Fig. 3). This suggests a possible route by which the cusp formation processes could be characterised and predictive models developed.

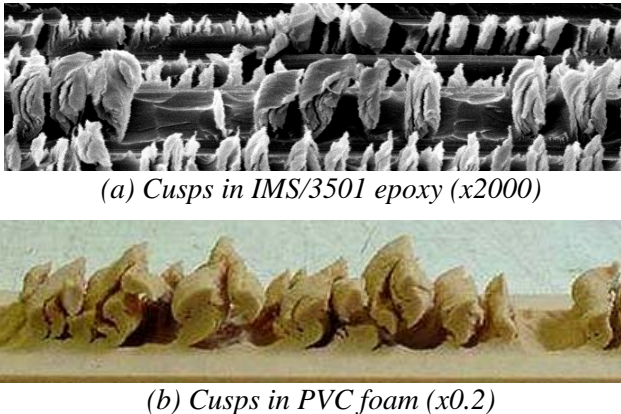


Fig. 3 Cusps in CFRP and PVC foam

The testing entailed loading PVC foam between two very stiff steel blocks under rail shear. For this study, the ASTM standard test method C-273 [11] was followed using Divinycell H200 PVC foam ($\rho=200\text{kg/m}^3$, $\tau_{12}=3.5\text{MPa}$, $G_{12}=85\text{MPa}$) [12]. The specimen length, width and thickness were 300mm, 75mm and 25mm respectively. The cross-section profile was varied to characterise its influence upon cusp formation. The baseline condition followed the ASTM standard with 12mm deep U-shaped channels machined either side of the foam. Two other profiles were considered; square profile channels (10mm deep) and plain (non-machined). The PVC foam was machined to size and then bonded between the steel blocks using Araldite 420. All the tests were carried out at room temperature using a 100kN Instron screw driven machine at a displacement rate of 3mm/min. Throughout testing load-displacement data was collected as well as measurements of the strain in the side faces of the foam, using Digital Speckle Photogrammetry (DSP) [13]. DSP is a full-field, non-contact strain measurement method and was used to quantify the strain field during the cusp formation process. As well as the observations from the tests to characterize the processes of cusp formation, these tests also provide validation for predictive models (both analytical and numerical) which simulate the foam fracture processes. These models are being extended to model the behaviour

of the interply resin layer during delamination in laminated composites. Finally, it should be noted that the load-deflection response provides the basis of a traction law for interface elements [2].

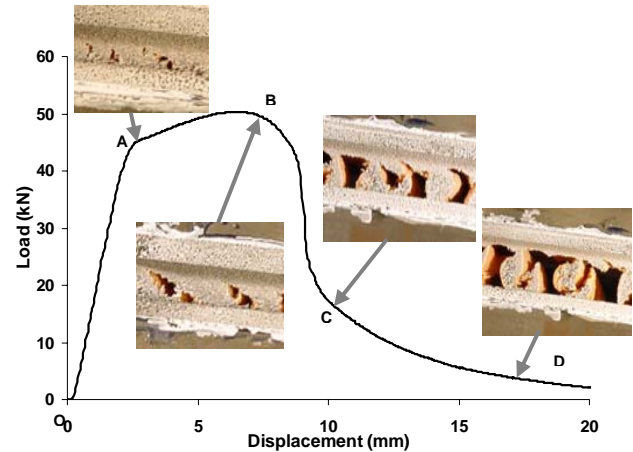


Fig. 4 Load-deflection response & cusp development of PVC foam (baseline) under shear

Fig. 4 shows the load/displacement response of the baseline (U-shaped channels) specimen, with snapshots of the fracture morphology also shown. The initial response was linear, until at point A there was a significant change in slope. From this point onwards, initiation of the angled cracks was observed at the edge of the foam, each initiating from the mid-thickness. These cracks propagated towards the interface between the foam and the steel substrate as the test progressed. The load continued to increase linearly albeit with a much reduced stiffness (between points A to B), and more cracks developed between those which had initially formed, up to the point of crack saturation (point B). The load then began to decrease and the cracks opened until the final phase of the process was reached (point C). During this final phase (CD in Fig. 4), the features rolled over and detached to form the cusps.

One valuable insight which these tests provide is the energy contributions to the toughness during each phase of the cusp development process. By considering the area under the load/displacement graph for each phase, the energy contributions can be deduced. The two key phases under consideration (Fig. 4) were OAB (crack formation) and OBCD (cusp deformation and rollover). Depending on whether the unloading curve would return to zero or exhibit gross permanent set, the first phase (crack formation) accounted for 20% to 50% of the total energy expended during fracture. If these results can be extended to modelling the behaviour of cusp formation in laminates, it would suggest that G_{IIC} has significant contributions both from crack

formation (which can be deduced purely from knowledge of G_{IC}) [7] and from cusp deformation.

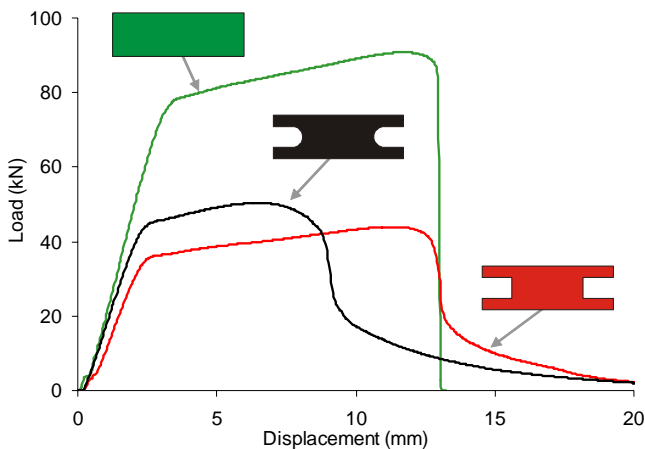


Fig. 5 Influence of foam specimen profile on load/displacement response of the shear test

Fig. 5 shows the influence of profile shape on the load-displacement response for three different profiles, namely those with a plain, square and U-shaped (baseline). The profile clearly altered both the overall fracture energy expended and the proportion expended during each phase, and also influenced the type of fracture. The plain profile specimen failed at the substrate/foam interface with small, undeformed cusps apparent. Consequently, the majority of the fracture energy (90%) was expended during the first phase. For the square profile specimen the cusps initiated close to the substrate/foam interface and were sharper and more numerous cusps than those in the baseline. Most of the energy was expended during the second phase (cusp deformation).

3 Multidirectional Ply Interfaces and Migration

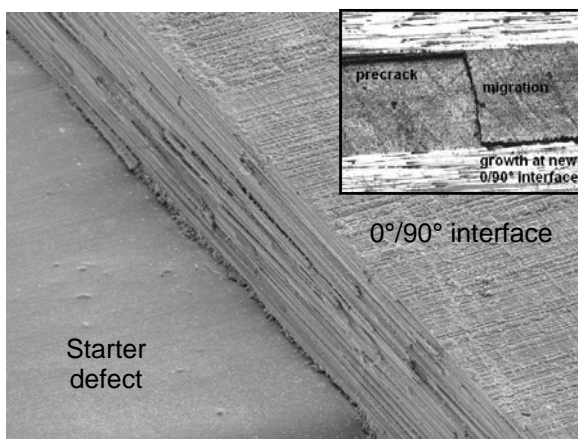


Fig. 6 Delamination migration at a $0^\circ/90^\circ$ ply interface in T800/924 (x200)

In structures, delaminations almost exclusively develop at non-zero ply interfaces, so why are toughness tests conducted on unidirectional laminates? One of the difficulties which has plagued delamination research has been the problems associated with characterising the toughness of multidirectional ply interfaces. When researchers [14] have attempted to characterise the toughness of such interfaces using conventional fracture toughness tests, the results have exhibited enormous scatter. The failures have been complicated, including multi-plane delamination, ply splitting and even fibre fracture, and have borne little resemblance to delamination fracture surfaces observed in structures.

The key difficulty has been migration of the delamination from the original defect plane, which has invalidated the test [14]. Consequently this has led to the adoption of unidirectional ply interface toughnesses for design. An example of this migration is shown in Fig. 6, which shows the initiation site for a delamination at a $0^\circ/90^\circ$ ply interface in a fracture toughness specimen. The flat region on the left is the starter insert at the midplane ($0^\circ/90^\circ$ ply interface), and the delamination on the right is between a 0° and the midplane 90° ply. Bounding these regions is a ply split, extending through the thickness of the 90° ply. Clearly, the delamination has migrated into a different ply interface ($90^\circ/0^\circ$ interface), which means the test is no longer characterising the interface of interest (the midplane $0^\circ/90^\circ$ ply interface), and the differing arm thicknesses means the data reduction to calculate the critical strain energy release rate (G_C) is no longer valid. This would imply that the toughness values from such tests are not representative of those in real structures. Furthermore, when characterising $0^\circ/0^\circ$ ply interfaces, the plies tend to nest during processing. This promotes the development of fibre bridging during testing, which dramatically increases the apparent toughness. Such nesting, and thus fibre bridging, does not develop at multidirectional ply interfaces. Indeed the interply resin layer is considerably deeper in multidirectional ply interfaces and it has been demonstrated that composite toughness is very sensitive to this thickness [15]. Finally, the stacking sequence will also influence the apparent toughness of the interface because the residual stresses will differ from those in unidirectional laminates. All these factors call into question the validity of using $0^\circ/0^\circ$ interface data to deduce $0^\circ/\phi$ ply interface toughnesses in structures.

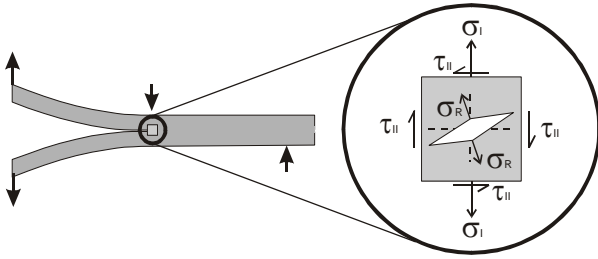


Fig. 7 Generalised stress state at the tip of a delamination under mixed-mode loading

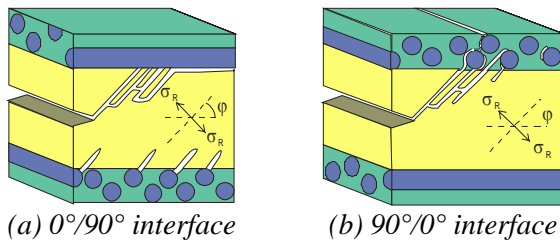


Fig. 8 Delamination mechanisms at a ply interface under mixed-mode loading shown in Fig. 7 (growth direction left to right)

To understand and overcome these difficulties, the mechanisms by which delaminations migrate in multidirectional laminates need to be understood. Migration can be explained by considering the resolved tensile stress, σ_R , due to the combination of shear and peel stresses at this site [1], as shown in Fig. 7. Under mixed-mode or mode II conditions, the resolved stress (and thus the crack front) is orientated out of the laminate plane. This means there is a natural tendency for the delamination to propagate out of the defect plane and migrate ‘upward’ towards the compressive face of the entire laminate under bending. If this migration is towards a ply in which the fibres are aligned with the normal to the delamination front (i.e. parallel to the driving force), the delamination will remain within the original defect plane and the interlaminar toughness can be characterized (Fig. 8a). However, if the ply orientation is not aligned with this direction (Fig. 8b), ply splitting will develop, and the delamination will migrate into the next ply interface. Ultimately, the delamination will migrate through the laminate until it reaches an interface in which the ply is orientated approximately parallel to the driving force. An interesting consequence of this mechanism is that it does not hold for pure mode I fracture since resolved stress is orthogonal to the laminate plane. Under these conditions, it has been observed that the crack plane tends to wander above and below the original defect plane [14].

This understanding of the migration mechanism leads to an approach for characterising multidirectional ply interfaces. An important consequence of this mechanism is that delaminations tend to grow within interfaces in which one ply is orientated in the growth direction. For the mixed-mode fracture toughness test shown in Fig. 7 (MMB), this is the uppermost ply at the defect plane. Therefore, the fracture toughness of a ply interface can be characterized by ensuring the 0° ply on the uppermost face. The implication of this is that only $0^\circ/\phi$ interfaces can be characterized. If both plies are not parallel to the driving force (i.e. parallel to the toughness specimen length), such as a $+45^\circ/-45^\circ$ ply interface, then the delamination will tend to migrate. Some researchers have managed to grow delaminations at such interfaces [16] but inspection of the fracture surfaces reveals that, locally, the crack growth direction was not parallel to the specimen length, but grew diagonally along the angle ply directions.

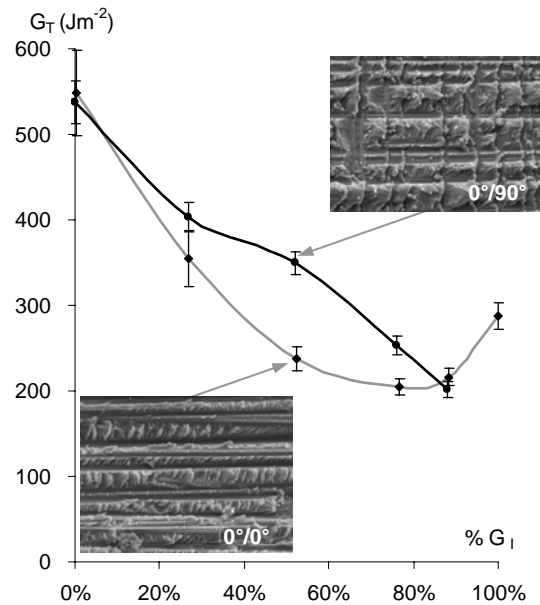


Fig. 9 Failure loci for $0^\circ/0^\circ$ and $0^\circ/90^\circ$ ply interfaces for T800/924

The toughness of $0^\circ/90^\circ$ and $0^\circ/45^\circ$ ply interfaces have been characterised by ensuring the 0° ply is uppermost. An example of the failure loci for $0^\circ/0^\circ$ and $0^\circ/90^\circ$ ply interfaces in T800/924 is shown in Fig. 9 [1,6]. The stacking sequence of the unidirectional ply interface was $[0^\circ_{24}]$ whilst the stacking sequence of the $0^\circ/90^\circ$ was $[(90^\circ, -45^\circ, +45^\circ, 0^\circ)_S(90^\circ, \pm 45^\circ, 0^\circ)_S(0^\circ, \pm 45^\circ, 90^\circ)_S(0^\circ, -45^\circ, +45^\circ, 90^\circ)_S]$. In addition, the fracture morphologies for these ply interfaces under 50% mode I loading is also shown.

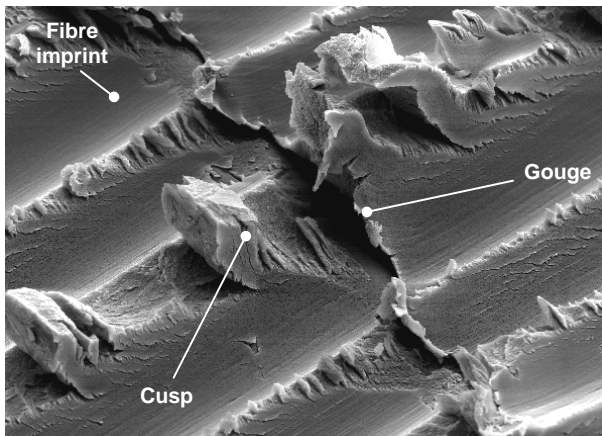


Fig. 10 Detail of a deep gouge at a $0^\circ/90^\circ$ ply interface under mixed-mode loading ($\times 5k$)

Under mode I dominated loading there is evidence that the toughness of the ply interfaces are similar, which is also reflected in the fracture morphology. However, as the mode II component increases, deep gouges ('ribs') develop on the fracture surface (Fig. 10). This fracture mechanism is not apparent at unidirectional ply interfaces and manifests itself as an increase in the toughness of the multidirectional ply interface. Again this suggests that using $0^\circ/0^\circ$ ply interface data to design for delamination in multidirectional structures is questionable, albeit conservative.

4 Delamination Growth in Structures

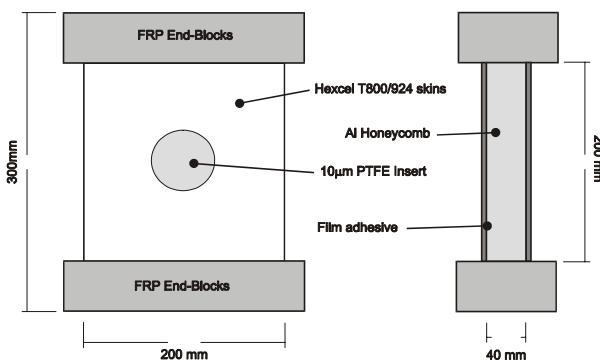


Fig. 11 Embedded defect element

The migration mechanisms in coupons described in the previous Section have important implications for delamination growth from embedded defects in flat laminates and structures. A number of researchers have investigated delamination growth from embedded defects in laminates, and numerous studies have attempted to model the delamination evolution [1]. However, many of these models have had limited success, particularly in attempting to model significant

delamination growth. The author has investigated the influence of delamination growth from embedded defects [17]. Laminates, 3mm thick, were manufactured from Hexcel T800/924 carbon/epoxy with a quasi-isotropic lay-up of $[(\pm 45^\circ/0^\circ/90^\circ)_3]_s$. A defect consisting of a $10\mu\text{m}$ thick PTFE film was included, at a depth either of 3 plies ($0^\circ/90^\circ$ interface) or 5 plies ($+45^\circ/-45^\circ$ interface). The laminates were supported using an aluminium honeycomb core (Fig. 11) to form sandwich panels. These panels were stabilised against buckling to strains up to $-10000\mu\epsilon$, eliminating the need for an anti-buckling guide and the associated complications [1]. The damage growth was monitored using calibrated shadow Moiré interferometry. The panels were loaded in compression at a rate of 0.3mm/min until the damage had approached the panel edges. After testing, the panels were ultrasonically scanned to determine the damage extent, and the fracture surfaces were dissected and examined using electron microscopy. Detailed fractographic analysis was conducted to characterise the damage mechanisms. A range of defect sizes and shapes were characterised, but the controlling factor for the delamination mechanisms was found to be the depth (and ply interface) of the initial defect. Therefore, for clarity, only the results for the 50mm diameter defects are reported here.

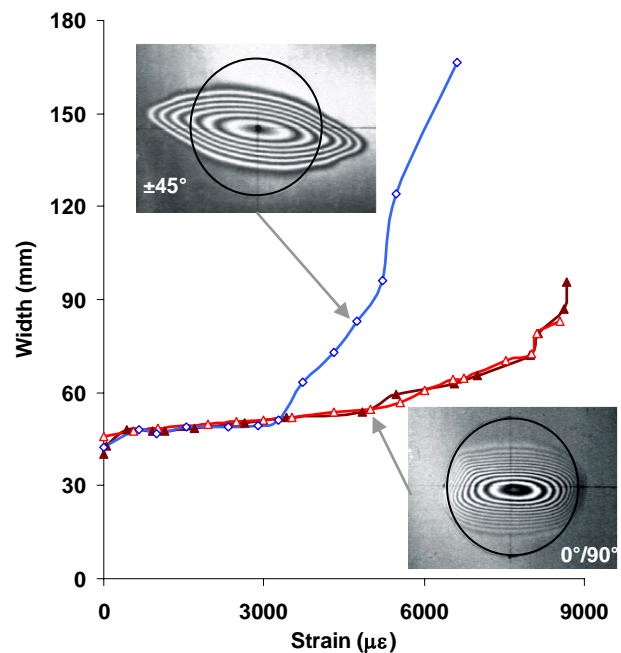


Fig. 12 Damage width versus applied strain, with a snapshot of the damage extent at $-5000\mu\epsilon$

Fig. 12 shows the damage width against applied strain for 50mm embedded defects at $0^\circ/90^\circ$

(3/4) and +45°/-45° (5/6) ply interfaces. Two nominally identical examples of the former are shown in the Figure. In addition, a snapshot of the delamination extent at an applied strain of -5000 $\mu\epsilon$ (with the initial extent indicated) is also shown. Firstly consider the shallower defect (0°/90° ply interface). As the load was introduced, the delaminated region buckled to form an elliptical blister. Delamination growth initiated from the ends of the major axis of this blister at an applied strain of about -2100 $\mu\epsilon$. The delamination formed a lozenge shape, with lobes growing on the right side, from just above the major axis of the blister and, on the left side, from just below the major axis, nearly parallel to the -45° ply. Secondary growth then initiated from the transverse boundary of the damage and propagated parallel to the +45° ply. The delamination developed into rectangular shape and, at an applied strain in excess of -6000 $\mu\epsilon$, into a dog bone shape. This led to rapid growth of the corner lobes, followed by splitting of the surface plies. Finally, at applied strains in excess of -8500 $\mu\epsilon$, there was longitudinal damage growth from the axial boundary of the insert. This damage evolution appeared to be very reproducible (Fig. 12).

The behaviour of the delamination growth from the deeper defect (+45°/-45° ply interface) was very different. As the load was applied, the delaminated region buckled into an elliptical blister, with the major axis orientated at 105° (clockwise) to the loading direction. At an applied strain of about -3100 $\mu\epsilon$ delamination growth initiated at opposing points on the defect boundary at about 100° to the loading direction. The delamination extended from these sites (as slip-stick growth), rapidly developing into a flattened ellipse until the tests were stopped at an applied strains of about -6000 $\mu\epsilon$. As can be seen in Fig. 12, the damage growth from the deeper defect was much more rapid than that from the shallow defect.

The observed damage growth could be interpreted in light of the migration mechanisms described in the previous Section. The fracture surfaces of the panel containing the 50mm circular defect located at the 0°/90° ply interface after the delaminated plies have been removed is shown in Fig. 13a. Fig. 13b is a micrograph of part of the delaminated material matching the surface from the substrate in Fig. 13a and illustrates the different damage planes and failure modes. On the application of the applied loads, the delaminated layers buckled, leading to peak delaminating conditions at the transverse extent of the defect boundary. However, due to the stiffness coupling of the unbalanced delaminated layers, the sites of these peak conditions were rotated slightly. The driving force for the delamination growth was orientated only approximately parallel to the 90° ply. Therefore, for the crack tip at the delamination initiation site, at the transverse extents of the defect, locally the upper ply was orientated at 90° and the lower ply at 0°. However, the shearing directions at the crack tip were the same as those shown in Fig. 7; i.e. the delamination would tend to be driven upward. As observed in coupons, this led to migration of the delamination to the next interface (0°/-45°). As had been previously observed in fracture toughness testing of $\pm 45^\circ$ ply interfaces [16] since there was a component of the driving force in the angle ply direction (-45°), some delamination growth consequently developed at this ply interface. These were the first lobes of the delamination observed in the tests. However, this still led to migration through this -45° ply into the next interface (-45°/+45°). Consequently, the delamination extended along the +45°/-45° interface, parallel to the +45° ply in this instance. This led to the second stage of the observed growth, leading to the dogbone shaped

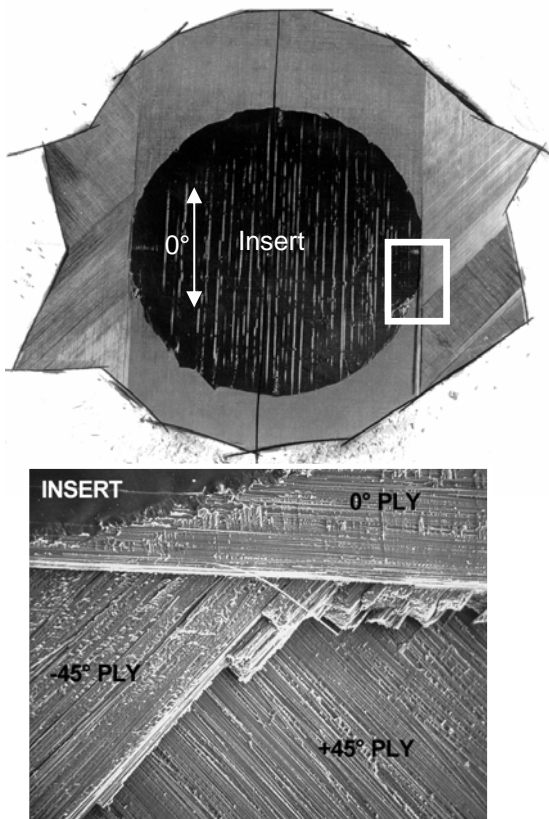


Fig. 13 (a) Fracture surfaces from 50mm defect at 0°/90° ply interface; (b) Detail of boxed area (matching fracture surface) (x500)

delamination extent late in the test. Ultimately, splits developed in the surface ply which alleviated the local driving forces at the crack tip and arrested the damage growth. The key observations here were that the delamination never encountered an interface in which the driving force and upper ply orientation were aligned. Consequently migration was promoted, which actually inhibited rapid growth.

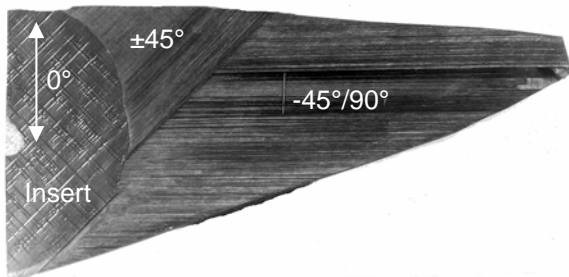


Fig. 14 Exposed fracture surfaces from the 50mm defect at the $+45^\circ/-45^\circ$ ply interface

For the deeper embedded defect ($\pm 45^\circ$ ply interface) the mechanisms were very different. The exposed delaminated plies are shown in Fig. 14; the delamination had to be sectioned in half to allow it to be exposed without damaging the growth sites. As with the earlier defect, the originally circular defect buckled into an elliptical blister, with the peak delamination conditions again at the transverse extents. The stiffness coupling was more severe in these delaminated layers than in the shallow defect, so the rotation of the site of the peak delaminating forces was greater. As can be seen in Fig. 14, unlike the shallow defect, the delamination growth initiated at the defect plane and extended parallel the $+45^\circ$ ply. However, as the delamination extended, the orientation of the delamination front deviated from being perpendicular to the driving force. Consequently, delamination migrated through the $+45^\circ$ ply, into the adjacent interface ($+45^\circ/90^\circ$). At this ply interface the conditions for delamination growth had been met; the upper ply and the driving force for the delamination were parallel. Consequently, there was rapid delamination growth within this ply interface, as can be seen in Fig. 12.

The key finding here was that the siting of the defect plane and the stacking sequence of the delaminated plies dictated the subsequent behaviour. The critical mechanism was delamination migration through the layers until an interface was reached in which the upper plies and driving force were coincident. In this example, the whole laminate was constrained such that it was always under membrane compression loading, and there was no global

bending of the laminate. Consequently, the orientation of the shear at the defect boundary was as shown in Fig. 7, and this led to the delamination migrating upwards.

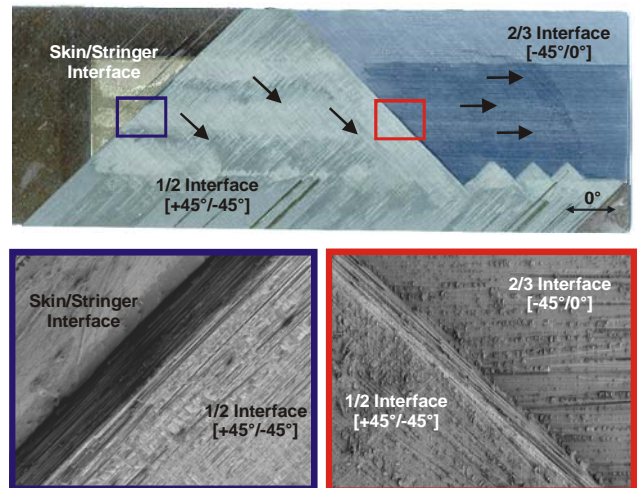


Fig. 15 (a) Failed stiffener runout; (b) skin delamination with migration sites shown ($\times 200$)

A further example of the migration mechanism controlling the growth (and failure) processes is shown in Figure 15 [18]. This example is from a stiffener run-out element, of skin stacking sequence $(\pm 45^\circ/0^\circ/90^\circ)_{3S}$, which had been loaded to failure in tension. Fig. 15 shows the exposed skin delamination, with the different interfaces marked, and electron micrographs of the migration sites. Under loading a delamination initiated at the tip of the stiffener (the left side of Fig. 15) with the driving force parallel to the stiffener length (and the shear orientated such that the migration drove into the skin). However, the skin/stiffener interface was $+45^\circ/+45^\circ$ (not aligned with the driving force), so the delamination migrated through the layers into the skin until it reached a $-45^\circ/0^\circ$ interface, at which it remained. The splitting and migration mechanisms observed were identical to those seen earlier [1].

The migration direction is influenced by the local shear orientation; when there is global bending, the direction of migration can thus be influenced, as presented in this last example of delamination growth in a post-buckled stiffened panel [19]. The panel was fabricated from HTA/6376C, with a 3mm thick quasi-isotropic skin $[+45^\circ/-45^\circ/0^\circ/90^\circ]_{3S}$ of length of 450mm. The panel had three I-section stringers (55mm wide footprint) on one face with a pitch of 150mm; the stringers were cured separately, and then cobonded to the skin. The skin contained a 40mm diameter PTFE defect in the centre of a bay between plies 4 and 5 ($90^\circ/+45^\circ$) closest to the stringer face. The panel was tested in quasi-static

compression to failure, although the test was interrupted to monitor the damage extent using ultrasonics. The panel buckled at $-2800\mu\epsilon$, with defect centre being coincident with a buckle antinode, following which transverse delamination growth developed from the lateral extent of the defect. This was similar to that observed in the element tests (Fig. 12), except the damage extent was not symmetrical (Fig. 16). Failure occurred at an applied strain of $-5523\mu\epsilon$ by stiffener debonding.

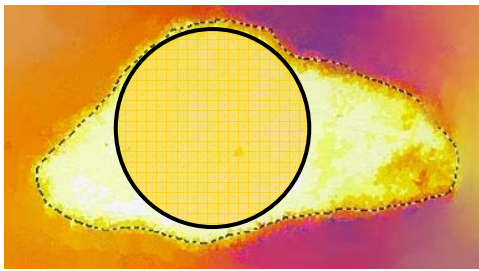


Fig. 16 Ultrasonic images of the initial (black) and subsequent delamination extent at $-5255\mu\epsilon$

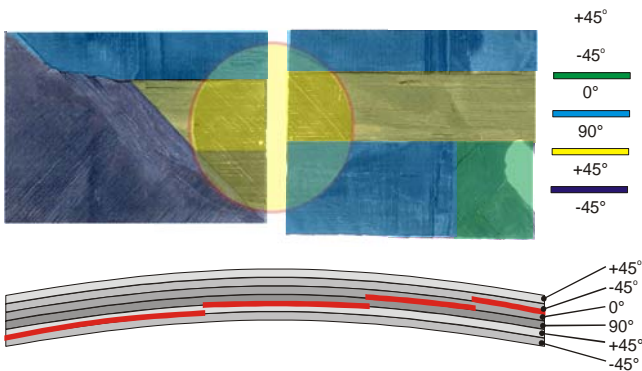


Fig. 17 Illustration of the delamination migration processes in the stiffened panel

Fig. 17 shows the exposed fracture surfaces, with the different colours corresponding to the different ply interfaces. The original defect plane ($90^\circ/+45^\circ$) is shown in yellow, below which is a $+45^\circ/-45^\circ$ interface, shown in blue. The interfaces above the defect plane are shown in light blue ($0^\circ/90^\circ$) and green ($-45^\circ/0^\circ$). Below the image of a fracture surfaces, an illustration of the general location of the delamination is shown in red. It is apparent that this differs to the fracture morphology for the embedded defects shown in Fig. 13. Most notably, the embedded defect under membrane compression (Fig. 13) exhibited rotational symmetry, whilst the delamination extent in Fig. 17 did not. In particular, the direction of migration was different either side of the defect. Towards the right hand side, the delamination has migrated upwards

towards the stiffener face of the panel, whilst on the left side it has migrated downwards, into the skin.

This difference in migration direction can be attributed to the change in the sense of the interlaminar shear either side of the defect. Because the defect was sited at a buckle antinode, on the right hand side the shear direction was such that the delamination migrated upwards towards the stiffener face of the panel, so the orientation of the uppermost ply of the interface controlled the migration process. On the other hand, on the left hand side, the orientation of the lowermost ply of the interface controlled the migration. Consequently, on the right hand side, the uppermost 90° ply at the defect plane led to rapid delamination extension towards the stiffener. However, on the left hand side, the lowermost $+45^\circ$ ply at the defect plane led to migration deeper into the laminate and thus inhibited growth. Importantly, the delamination on the right hand side reached the stiffener before that on the left hand side, and directly contributed to debonding of the stiffener and structural failure. This example demonstrates that the migration process is not only influenced by the stacking sequence, but also by the global stress state of the structure. Clearly, this migration mechanism is critical in dictating the behaviour of delaminated structures.

5 Implications and Concluding Remarks

Over the last few decades an enormous amount of research effort has been expended trying to address the problem of delamination. There are a range of failure criteria which have been proposed but most of these have little physical basis. Fractography provides a valuable insight into the link between fracture mechanisms and delamination toughness, and can assist in the development of physically based failure criteria. In conjunction with macroscale cusp tests, it can validate models for the contribution that cusp formation and deformation make to the overall delamination toughness. These tests also provide a generic traction law which can be utilised for interface element formulation.

Migration dictates the delamination growth processes. At a coupon level, by addressing migration, it is feasible to characterise the fracture toughness of $0^\circ/\phi$ ply interfaces. There is evidence that additional micromechanisms develop at these interfaces, thus leading to an increase in toughness. The implication is that the toughness of $0^\circ/0^\circ$ ply interfaces are not representative of those in structures, but do perhaps provide a conservative measure. An important consequence of this process

is that delamination toughness need not be characterized over a spectrum of ply orientations. For the $[\pm 45^\circ/0^\circ/90^\circ]$ laminates, only the toughness of $0^\circ/45^\circ$ and $0^\circ/90^\circ$ ply interfaces need to be determined to fully characterise delamination behaviour in structures. In structures delaminations preferably grow parallel to either the upper or lower ply at an interface; which ply depends upon the orientation of the shear. If driven to propagate at an interface not so aligned, migration develops and the delamination will change plane. This behaviour controls the global damage growth and is more critical than defect size or shape to the behaviour.

Regarding delamination modelling, a consequence of migration is that treating the delamination as remaining within the original defect plane is invalid. Furthermore, as shown in Fig. 14, assuming delamination growth is normal to the defect boundary (i.e. is self-similar) is also invalid. This requires revision of the formulation of G_I , G_{II} and G_{III} for virtual crack closure calculations [20]. Consequently, modelling of a relatively simple starter defect (such as a single plane defect) can lead to very complex mechanisms, particularly at large crack lengths. Predictive models need to incorporate procedures for multiphase growth and intralaminar fracture. Ironically, for a complex initial damage state, such as from low velocity impact, the growth processes may be simpler, since delamination will already be located at the critical ply interface and thus migration may not occur.

The effects described here offer a route for damage tolerant design of composite structures; i.e. to inhibit delamination growth, migration should be promoted (Fig. 13). For example, in laminates under compression loading, the delamination will preferential grow at interfaces with plies transverse to the loading direction. Therefore, these plies should be positioned such that the delamination will not migrate to a critical interface. However, the global loading conditions at the defect will also influence the migration conditions. Growth and migration rules can be exploited to tailor the stacking-sequence for damage tolerant design.

6 References

- Greenhalgh, E., "Characterisation of mixed-mode delamination growth in carbon-fibre composites", PhD Thesis, Imperial College, UK, (1998).
- Pinho S., Iannucci L., Robinson P., "Formulation & implementation of decohesion elements in an explicit finite element code", *Composites A*, Vol. 37, pp 778–789, (2006).
- Reeder J.R., "An evaluation of mixed-mode delamination failure criteria", NASA Langley Research Center, *NASA TM 104210*, (1992)
- Xia Z.C., Hutchinson J.W., "Mode-II Fracture-Toughness of A Brittle Adhesive Layer", *Int Journal of Solids & Structures*, Vol 31, pp1133-1148, (1994)
- Fleck N.A., "Brittle fracture due to an array of microcracks", *Proc. Roy. Soc.*, A432, pp55-76, (1991)
- Greenhalgh E.S., Asp L., Singh S. "Delamination Resistance, Failure Criteria and Fracture Morphology of 0/0, 0/5 and 0/90 Ply Interfaces in CFRP". 1999 Mar 18; *5th Int Conf on Deformation & Fracture of Composites*, IMechE, London, UK, (1999)
- O'Brien, T. K., "Composite interlaminar shear fracture toughness, G_{IIC} : Shear measurement or Shear Myth?", *American Society for Testing and Materials*, ASTM STP 1330, Philadelphia, pp3 – 18, (1998)
- Kinloch A.J *et al*, "The Mixed-Mode Delamination of Fibre Composite Materials", *Composites Sci & Tech*, Vol 47, pp225-37, (1993)
- Jelf P.M., Fleck N.A., "Compression Failure Mechanisms in Unidirectional Composites", *J of Composite Materials*; Vol 26, pp2706-2726, (1992)
- Asp, L., Sicomp, Sweden, Communication, (2006)
- ASTMC-273, "Standard test for shear properties of sandwich core materials", ASTM, (2006)
- http://www.diabgroup.com/americas/u_literature/u_pdf_files/u_ds_pdf/H_DS_U.pdf, (2007)
- <http://www.gom.com/EN/measuring.systems/aramis/system/system.html>, (2007)
- Andersons J., Konig M., "Dependence of fracture toughness of composite laminates on interface ply orientations and delamination growth direction", *Comp Sci & Tech*, Vol. 64, pp2139-2152, (2004)
- Datta S, "Investigation of the micromechanics of delamination in fibre reinforced composites", PhD Thesis, Imperial College, UK, (2005)
- Robinson P, Song D, "A Modified DCB Specimen For Mode-I Testing Of Multidirectional Laminates", *J Compos Mater*, Vol 26, pp1554 - 1577, (1992)
- Greenhalgh E, Singh, S, "Investigation of the Failure Mechanisms for Delamination Growth From Embedded Defects", *ICCM 12*, Paris, France, (1999)
- Greenhalgh E, Garcia, M, "Fracture mechanisms and failure processes at stiffener run-outs in polymer matrix composite stiffened elements", *Composites Part A*, Vol. 35, pp1447 - 1458, (2004)
- Greenhalgh, E.S, Meeks, C.B, Clarke, A.B., Thatcher, J.E., "The Effect of Defects on the Performance of Post-Buckled CFRP Stringer-Stiffened Panels", *Composites A*, Vol. 34, pp623-633, (2003)
- Lord, S.J, Greenhalgh, E.S., "Modelling of Delamination and Debonding in Laminated Composites using a Moving Mesh Approach", *11th European Conference on Composite Materials*, Rhodes, Greece, (2004)